DOI: 10.1021/cg901104j

CRYSTAL GROWTH & DESIGN Article

2010, Vol. 10
1585–1589

ZnO Nanowire Growth: A Deeper Understanding Based on Simulations and Controlled Oxygen Experiments

Kittitat Subannajui,*,† Niranjan Ramgir,*,† Raphael Grimm,† Rebecca Michiels,† Yang Yang,‡ Stefan Müller,§ and Margit Zacharias†

†*Institute of Microsystems Engineering, University of Freiburg, Georges-Koehler-Allee 103, 79110 Freiburg, Germany,* ‡*Max Planck Institute of Microstructure Physics, Weinberg 2, 06120 Halle, Germany, and* §*Fraunhofer Institute for Applied Solid State Physics, Tullastrasse 72, 79108 Freiburg, Germany*

Received September 9, 2009; Revised Manuscript Received January 14, 2010

Ⓦ **This paper contains enhanced objects available on the Internet at http://pubs.acs.org/crystal.**

ABSTRACT: A binary flow of a Ar/Zn mixture has been used in simulations as well as in physical growth experiments for ZnO nanowire growth by vapor phase deposition. Systematic investigations of the gas transport and the chemical behavior under controlled vacuum and flow conditions revealed that the gases emerging from carbothermal reduction, namely, $CO_{(g)}$ and $CO_{2(g)}$, are not enough to stimulate a controlled ZnO nanowire growth. An optimum O_2 concentration is crucial to promote nanowire growth, while $CO_{(g)}$ and $CO_{2(g)}$ enhance the tendency to grow a film. Importantly, the here presented simulations can be used to predict and tailor the region of nanowire growth under appropriate assumptions for any tube furnace.

Introduction

The size reduction of electronic devices by photolithography is limited, and the properties of etched one-dimensional (1-D) structures are very often disturbed by the nonperfect surface. A much better way is the direct growth of nanostructures at desired positions with suitable arrangements such as a nanowire (NW) arrays. Today's nanotechnology is focusing on attempts to obtain semiconductor devices based for instance on NWs of different materials.[1] Several materials have been demonstrated for such novel 1-D devices grown with an amazingly high perfection in crystallinity and a high device performance; examples are based on Si, Ge, II−VI, or III−V semiconductors. Of these, ZnO NWs have attracted a lot of attention due to the simplicity of fabrication using different processes and precursors and due to the observed encouraging electronic and optical properties. In comparison to GaN, ZnO has a band gap in a similar range (3.3−3.4 eV); however, its growth process is rather simple, and in most cases the resulting crystal quality is amazingly high. The NWs grow normally self-organized with a preferential growth direction along the *c*-axis (0001). Very high aspect ratio NWs and complex structures with interesting properties can easily be realized.[2,3]

Reproducibility in the growth processes is the minimum requirement for using the bottom-up NW technology in electronic and sensor applications.[4−6] However, such a reproducible growth has not been achieved so far, and most experiments are case studies with a limited control and understanding. Various processes such as metal organic chemical vapor deposition (MOCVD),[7] solution-phase process,[8] or vapor phase (VP) deposition have been used for the growth.[9] The vapor phase process has been the most often used for ZnO NWs. A number of papers reported on the growth process. Properties as well as applications of ZnO NWs were reported previously.[10,11] The VP process can be realized either as a vapor−liquid−solid (VLS) or as a vapor-solid (VS) process using appropriate conditions inside a horizontal tube furnace. The growth is known to be very sensitive toward parameters such as source type, substrate orientation, size of catalyst, temperature or temperature profile of the tube furnace, partial pressure of reactants and gas flow, and last but not least the geometry of the tube furnace. It was reported earlier that the NWs can be grown on various positions inside the tube including at upstream positions.[12,13] And only the upstream position offers the possibility to study the influence of oxygen separately and under a limited involvement of the carbothermal reduction products, namely, the $CO_{(g)}$ and $CO_{2(g)}$. The so-called carbothermal reduction relies on the reaction of the ZnO and graphite to produce $Zn_{(g)}$ and $CO_{(g)}$ being involved in a mixed state in the transported gas to react then at the NW growth position to ZnO and CO_2.[14,15] Recently, various reports on growth processes without carbothermal reduction implied that $CO_{(g)}$ might not be required for the growth at all.[16,17]

Up to now, modeling the gas flow during the NW growth and its dependence on the various parameters and furnace geometries was not reported to our knowledge. Most groups have used an empirical search for suitable growth conditions for their respective tube furnaces. Hence, a detailed understanding of NW growth from a kinetic and thermodynamic point of view is not available so far. In the here presented work, we concentrate on the fundamental concepts involved in VP deposition. We present a systematic study demonstrating the necessity of an optimum O_2 concentration for successful NW growth without a wetting layer. In order to clarify the growth mechanism, the role of both $CO_{(g)}$ and $O_{2(g)}$ was carefully studied enabling for the first time the separation of both. Using an upstream transport, the physical transport itself was thoroughly analyzed. The simulations demonstrated the estimated transport direction of the $Zn_{(g)}$ component in mixed gases. The results were used to determine and predict the growth to form films, NWs, or nuclei by precisely controlling the O_2 concentration inside the system. It will be shown that our experimental results are well supported by the here presented simulations.

*To whom correspondence should be addressed. E-mail: kittitat.subannajui@imtek.uni-freiburg.de.

Published on Web 02/26/2010

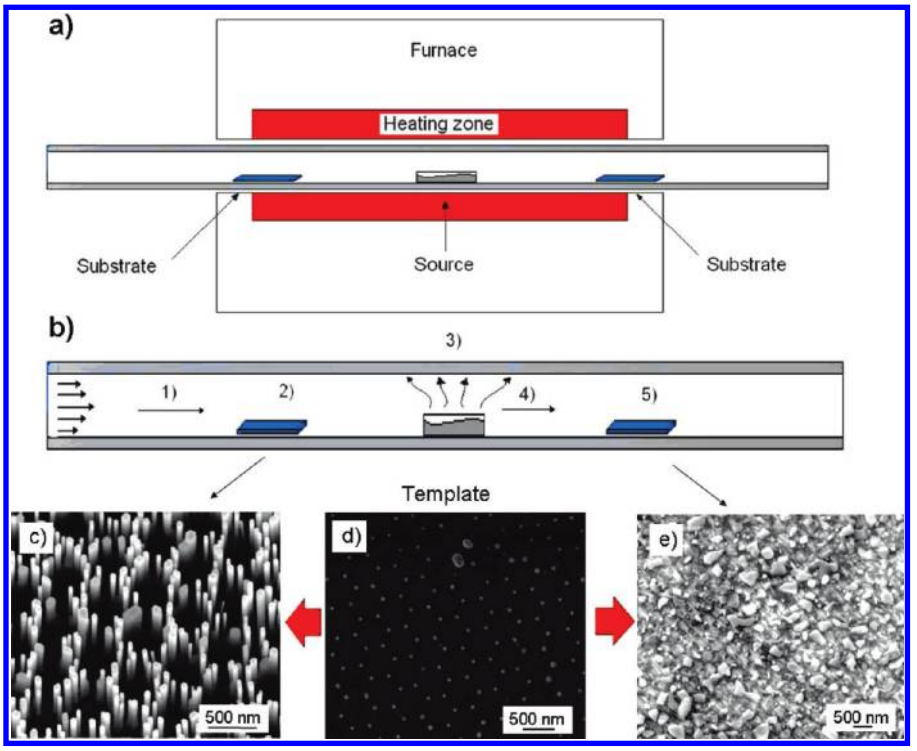

Figure 1. (a) Schematic of the experimental setup, (b) gas flow and reaction mapping inside the tube; numbers show the specific positions inside the tube as used in the paper. (c) NWs grown at position 2, (d) initial pattern before the growth experiment, (e) ZnOx film grown at position 5.

Experimental Section

ZnO NWs were grown by a vapor phase deposition on GaN/sapphire substrates containing hexagonal patterning of Au prepared by nanosphere lithography (NSL). In the present case, Au dots act as a position selecting catalysts on the substrates. As a source, ZnO powder (Alfa-Aesa ZnO 99.99%) and graphite (Alfa-Aesa -200 mesh) was mixed at a weight ratio of 1:1. The source powder (1.4 g) and two substrates were placed inside the horizontal 1-in. diameter tube furnace as shown in Figure 1a. The small tube diameter confined the gases and the reaction occurred homogeneously. Vacuum seals were firmly tightened to prevent any unwanted O_2 leaking in from the ambient, which is a crucial and often neglected parameter for the ZnO NW growth. A leak test was performed observing the change of static pressure inside the closed tube (200 mbar) overnight. The leakage rate was very small and undetectable. The input gas was flowing from left to right with the continuous flow of $Ar_{(g)}$ at a flow rate of 5 sccm. In addition, a very sensitive valve enabled adding oxygen in a controlled way ($O_{2(g)}$ at a flow rate of 0.001 ($\pm$0.0005) sccm). The tube was filled with a constant pressure of 200 mbar before starting the experiment. The growth temperature and heating duration were 930 °C and 10−20 min, respectively. NWs were characterized using scanning electron microscopy (Nova nanoSEM, FEI Company, Netherland) and transmission electron microscope coupled with selected area electron diffraction (SAED) patterns using Philips CM20T 200 kV. The gas flow inside the tube was designed and simulated using ANSYS CFX 11.0 software.

Results and Discussion

Figure 1a shows a schematic view of the experiment setup in which a quartz boat containing the source material was placed in the middle of the tube; Figure 1b indicates the position of the substrates containing the patterned Au arrays. The quartz boat hinders the gas flow especially in the present case where the inner diameter of the tube is 1 in. In Figure 1b the working zone (35 cm) of the horizontal tube is shown with more details. The growth at different places inside the tube furnace is summarized in Figure 1c,e. Figure 1c,e represents nanostructures observed at positions 2 and 5, respectively (in accordance with Figure 1b), while Figure 1d is an example of the used Au pattern on the substrate. Obviously, very different ZnO nanostructures were observed and the simulations presented below will help to interpret these results. The diameter of the ZnO NWs were around 50−60 nm and were single crystalline with a preferred orientation along [0001] as evident from Figure 2.

For the simulation, we assumed an isothermal tube wall of 930 °C, which is equal to the experimental temperature to simplify the thermal model. The tube wall temperature will contribute to increase the gas temperature due to thermal conductivity. It is hard to evaluate the exact amount of $Zn_{(g)}$ evaporated from the powder source. Knowing the temperature-dependent vapor pressure would give a hint. However, using ZnO and graphite as a source complicates the situation and no values are available for such a case. Therefore, as an estimation, the amount of $Zn_{(g)}$ is set approximately to 10^{-10} kg/s as was also observed from thermogravimetric investigations. The gas flowing inside the tube is a mixture containing several components such as $Ar_{(g)}$, $CO_{2(g)}$, $CO_{(g)}$, $Zn_{(g)}$, and eventually $O_{2(g)}$. In the present case, $Ar_{(g)}$ is used as the transport gas. Hence, $Ar_{(g)}$ will be present in much higher quantity than any of the other gases, and we can assume that the Reynolds number is depending solely on its flow. In the present flow case, the Reynolds number is less than 14 which is far below that of a turbulent condition (4000). Therefore, a laminar flow in the binary system (Zn−Ar) governed by the transport equation is assumed:

$$\frac{\partial \rho \Phi}{\partial t} + \nabla \cdot (\rho \vec{u} \Phi) = \nabla \cdot (\Gamma \nabla \Phi) + S \qquad (1)$$

ρ is the density of the mixture, $\vec{u}$ is the velocity field, Φ is the concentration, Γ is the diffusivity,[18] and S is the source term.

Figure 3 shows the simulated stream line inside the tube at 10 min for different flow rates of the carrier gas (5 s/step).

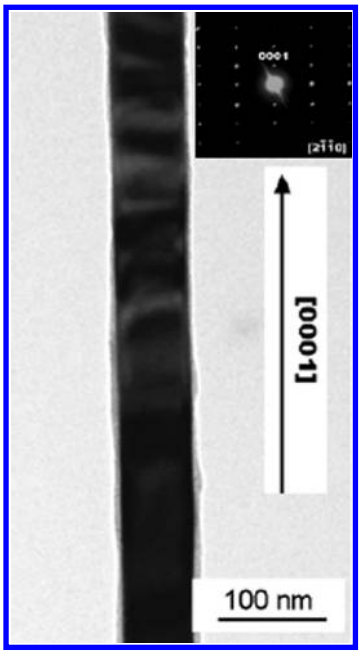

Figure 2. TEM results of ZnO NW exhibiting a growth direction along [0001].

When the mass flow is low, for example, 5 sccm, the stream line is coiling inside the tube. Once the flow rate is increased, the coiling of stream lines is reduced and the stream lines get more and more straight. This can be explained in terms of the continuity equation (which is one of the governing equations in ANSYS CFX)

$$\frac{\partial \rho}{\partial t} + \frac{\partial}{\partial x_j}(\rho \vec{u}_j) = 0 \qquad (2)$$

If the mass flow rate is reduced, then the second term in eq 2 is increased, thereby also increasing the velocity of the components. This result indicates that each gas molecule needs more space for moving inside the tube due to the increased velocity with a limited volume. Consequently, gas molecules circulate to a very nearby area implying an increase in the sticking probability as gas molecules pass many times the sample crucial for enhancing the deposition rate.

The net transport of Zn estimated from this simulation is shown in the Figure 4. In case of 5 sccm, $Zn_{(g)}$ gets distributed in both directions (left and right). The Zn concentration is higher on the right-hand side (downstream) because the carrier gas ($Ar_{(g)}$) is set to flow from left to right. However, $Zn_{(g)}$ is able to reach the left end of the tube in less than 1 min. The simulation result also corresponds to our experimental result. We observed that ZnO NWs can be grown on the left-hand side (upstream) of the tube within only 5 min or even less. With the increase of mass flow, the active area for growing ZnO NWs gets shifted to the right-hand side of the tube. The higher flow rate pushes the $Zn_{(g)}$, and therefore it will only partially reach the left-hand side. In other words, Zn transport against the gas flow becomes difficult with the increase in carrier gas flow rate. For example, when the mass flow rate is 50 sccm, only a very small part of Zn is transported to the left-hand side of the boat as observed in Figure 4c. Performing the experiment under various conditions, we observed the growth of the NWs in the actually predicted regions. This implies that the simulation results really help to

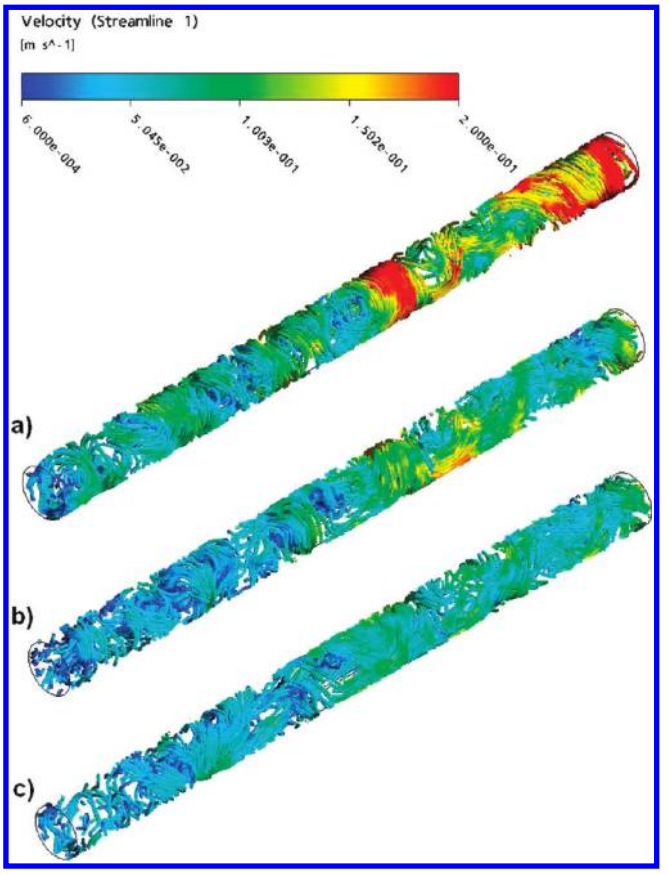

Figure 3. Ⓦ Stream line of the mixed gases inside the tube at 10 min for different flows of the carrier gas (a) 5 sccm, (b) 20 sccm, and (c) 50 sccm.

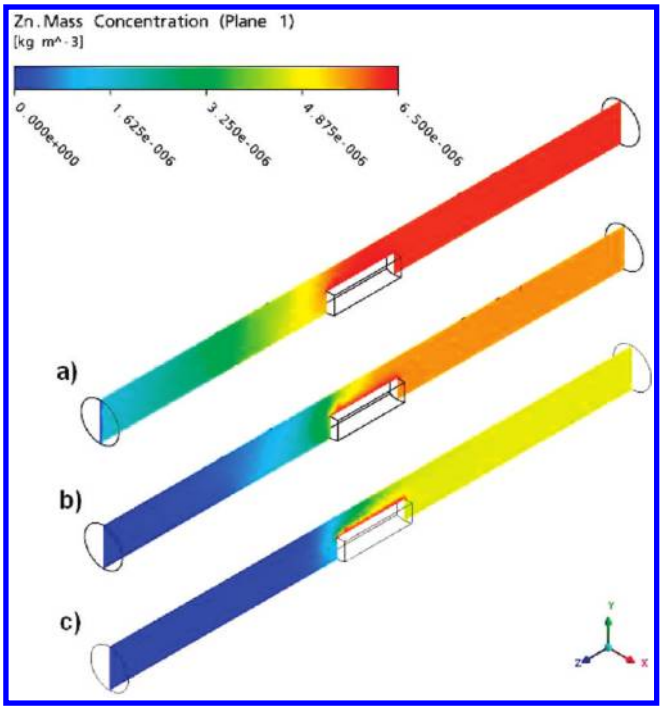

Figure 4. Ⓦ Simulated zinc distribution as a function of the gas flow estimated after the experiment proceeds for 10 min for Ar transport flow of (a) 5 sccm, (b) 20 sccm, and (c) 50 sccm.

predict the growth of NWs at different positions inside the experimental tube furnace system. Further, depending on the

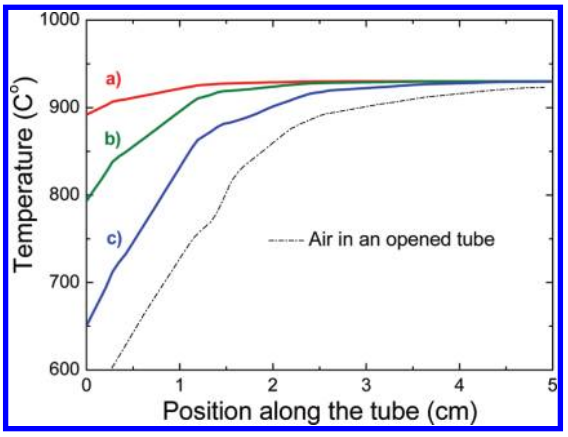

Figure 5. Temperature profile along the tube for varied flow rates: (a) 5 sccm (red line), (b) 20 sccm (green line), and (c) 50 sccm (blue line). Higher flow results in stepper temperature gradient. The dashed line represents the reference temperature profile of an open tube (air).

controlled mass flow, $Zn_{(g)}$ can even be transported to an upstream position.

In addition, the above results are well supported by the temperature mapping of the selected tube, which is another important factor for growing NWs. Of course, the chosen gas flow rate will affect the temperature profile of the tube and hence the optimum growth position of wires. Figure 5 shows the temperature profile obtained from simulations for different flow conditions. When the flow rate increases, the upstream temperature drop increases, too. A higher temperature gradient would be a disadvantage for the nanowire growth because the temperature on different substrate positions cannot be homogeneously controlled anymore.

At this point, we like to explain the result in terms of physical boundary conditions and chemical reactions inside the tube. It is well-known for the growth condition of ZnO NWs that the amount of all vapor phases has to be optimized. The growth mechanism depends on the competition between several gas phases. When the Ar gas flow is 5 sccm, its concentration inside the tube is high in comparison with other gas components that can be considered as minor constituents. The experiment was performed under semistatic flow conditions that allow the back transport of Zn vapor in Ar atmosphere (please see the simulation). If we now add (in a controlled way) a very small flow of $O_{2(g)}$ the oxygen will be slowly transported from the left to the right side of the tube, entering at the inlet and leaving at the outlet. Please note this can also happen unintentionally by having a leakage at the inlet seal. In our case, we used good vacuum conditions (no leaking) and introduced intentionally an O_2 gas input by a needle valve. There is no back diffusion of Zn vapor outside the heating zone since the temperature is much lower than its melting point. The small tube dimension (1 in. diameter) used here forces all gases to mix homogeneously. Referring to Figure 1b, the gases at the position 1 far outside the heating zone are only $Ar_{(g)}$ and $O_{2(g)}$ with no growth expected and observed. Shifting to position 2, where O_2 and $Zn_{(g)}$ will encounter each other, the condition is optimally suited for the growth of NWs, and we actually observed the growth of NW. The important reaction is (O_2 rich region).[19]

$$2Zn_{(g)} + O_{2(g)} \rightarrow 2ZnO_{(s)} \quad (3)$$

Equation 3 will be discussed as the dominant reaction later. When $O_{2(g)}$ reaches position 3, it meets the volume containing the product of the carbothermal reduction, that is,

$$ZnO_{(s)} + C_{(s)} \rightarrow Zn_{(g)} + CO_{(g)} \quad (4)$$

$$CO_{(g)} + ZnO_{(s)} \rightarrow CO_{2(g)} + Zn_{(g)} \quad (5)$$

Now, because the tube diameter is small and the gas flows slowly, most of the $O_{2(g)}$ reacts with $CO_{(g)}$ above the source container which might not be the case for a bigger tube or a higher flow rate. Hence, O_2 is depleted at position 4 and onward and the major reactions at this position 4 are (O_2 deficient or CO rich region)

$$C_{(s)} + CO_{2(g)} \rightarrow 2CO_{(g)} \quad (6)$$

$$2CO_{(g)} + O_{2(g)} \rightarrow 2CO_{2(g)} \quad (7)$$

At position 4, the sample next to the source, we observed uncompleted ZnO NWs because of the small remnant O_2 condition. At position 5, a Zn or ZnO_x film is grown under the O_2 depleted conditions (Figure 1e). In this $CO_{(g)}$ rich case, a large amount of $Zn_{(g)}$ molecules deposit on the substrate as $Zn_{(l)}$. The temperature at this region is rather low and the Zn vapor starts to wet the substrate to form liquid metal $Zn_{(l)}$, which afterward appears as Zn film without a proper oxidization due to the O_2 deficient condition. However, when the whole process stops and the furnace is cooling down, the carbothermal reduction also stops due to the temperature drop. The remaining O_2 is now free from the reaction with the product of the carbothermal reduction, and might oxidize the Zn film (ZnO_{1-x}) later. Hence, in a small tube as used here, the vapor phase process rather forms a film at the right-hand side (position 5).

In order to confirm the concept of ZnO NWs grown by reaction (3), we performed the same experiment using a low flow rate of only 5 sccm, but this time, additional $O_{2(g)}$ is provided also from the right-hand side by a controlled gas input installed at the outlet. Interestingly, the ZnO NWs now grow properly at position 5 as well. In other words, the growth condition is strongly influenced by the presence of additional $O_{2(g)}$ and a pronounced reaction following (3) takes place. Therefore, a region where formerly a ZnO_{1-x} film was observed is changed into a region of clear NWs growth; that is, NWs are now observed to grow in both position 5 as well as position 1. Overall, the experimental results provide a clear evidence and understanding of the growth of NWs.

In the last step, we studied the influence of $O_{2(g)}$ on the growth of ZnO NWs using the same left-hand side growth as above, but varying the O_2 concentration by using different partial flow rates of the $O_{2(g)}$. Figure 6a−c demonstrates the effect of the varied $O_{2(g)}$ flow. Obviously, the ZnO NWs can be grown best with an optimum O_2 concentration (Figure 6b); the amount might be different for other tube dimensions. On the other hand, under an insufficient or depleted O_2 condition, ZnO NWs are unable to grow, and Zn or ZnO_x films are formed instead (Figure 6a). These results again confirm the observation of different nanostructures between rich and poor $O_{2(g)}$ concentration as shown by the first experiment. For an excessive amount of $O_{2(g)}$, only nuclei are produced on the surface (Figure 6c). Most of the nuclei are round in shape as the original Au dots, but some nuclei form a hexagonal shape which indicates the crystallization of ZnO. The reason why the excessive amount of O_2 leads to ZnO_x dots (Figure 6c) rather than to the growth of ZnO NWs might be attributed to the fast oxidation of the condensing Zn gas. ZnO has a much higher melting point (1975 °C) than Zn (420 °C) and hence will

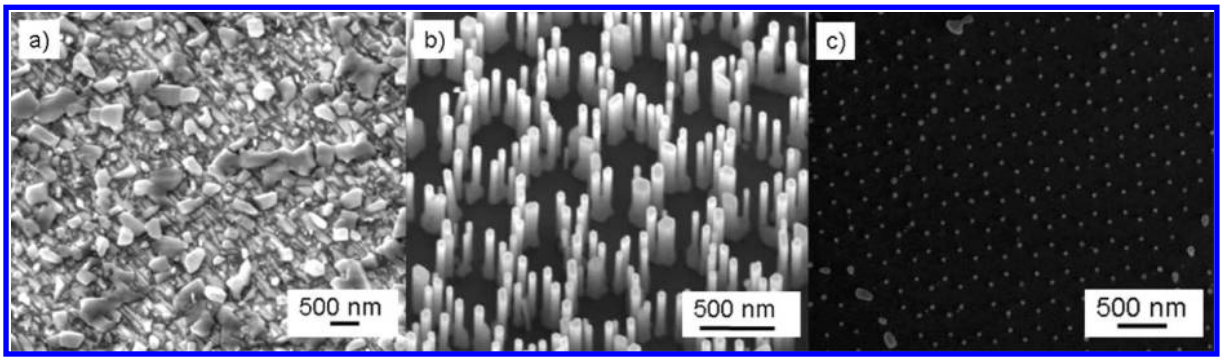

Figure 6. ZnO NWs grown at the position 2 with different O_2 flow rates (a) no oxygen, (b) limited oxygen of up to 0.001 sccm (10 degree tilt), and (c) higher than 0.01 sccm demonstrating the optimum O_2 for a successful wire growth.

immediately result in a solid interface. It was reported before that excessive O_2 might suppress the deposition rate or the surface diffusion.[20] In addition, the wetability,[21] sticking coefficient, and diffusivity of Zn atoms are higher than those of ZnO molecules. In principle, the sticking coefficient on a liquid surface is nearly 1, but if there is no liquid Zn anymore then there will also be no further ZnO growth under the very short growth times used in our experiments. Hence, it is possible that excessive O_2 decreases the deposition and the NWs growth. Also the additional oxygen might suppress the carbothermal reduction and the amount of $Zn_{(g)}$ is reduced at the end. Another way to understand this is by considering the standard Gibbs free energy of ZnO formation (eq 7) under equilibrium conditions for NWs growth that can be represented as

$$\Delta G^0 = -RT \ln K_{eq} \tag{8}$$

$$K_{eq} = \frac{1}{[Zn_{(g)}]^2[O_{2(g)}]} \tag{9}$$

where R is the gas constant, T is the temperature, and K_{eq} is the reaction equilibrium constant.

From the above equation it is clear that by drastically increasing the partial pressure of O_2, the Gibbs free energy (as also ZnO formation enthalpy) is greater, and the reaction can be hindered and vice versa.

Conclusion

In summary, the vapor phase deposition of ZnO NWs was investigated in detail. The transport direction and the distribution of $Zn_{(g)}$ was simulated using the data of a real tube furnace and compared with the respective growth experiments. As demonstrated here, the results can be used very well to predict the ZnO growth behavior of NWs and nucleated films. If the transport gas flow rate is sufficiently low, the system is in a steady state condition and $Zn_{(g)}$ is even able to be transported opposite to the flow in the upstream direction. When the flow rate increases, the $Zn_{(g)}$ gas is pushed into the transport gas flow direction. By using the advantage of a Zn transport to the left-hand side, we demonstrated the effect of $O_{2(g)}$ on the ZnO NWs grown at upstream and downstream positions. We demonstrated that by increasing the O_2 concentration inside the system one can control the growth from a film into NWs. For the first time simulations coupled with chemical behavior investigation were used to understand the growth of ZnO NWs. Our results further indicate that an optimum flux of $O_{2(g)}$ is crucial for ZnO NWs growth.

Acknowledgment. K.S. and M.Z. acknowledge financial support from DFG research contracts ZA 191/17. N.S.R. acknowledges the AvH Humboldt Foundation for a fellowship.

References

(1) Fan, Z.; Ho, J. C.; Jacobson, Z. A.; Razavi, H.; Javey, A. *Proc. Natl. Acad. Sci. U.S.A.* **2008**, *105*, 11066–11070.
(2) Klingshirn, C. *Chem. Phys. Chem.* **2007**, *8*, 782–803.
(3) Tian, Z. R.; Voigt, J. A.; Liu, J.; Mckenzie, B.; Mcdermott, M. J.; Rodriguez, M. A.; Konishi, H.; Xu, H. *Nat. Mater.* **2003**, *2*, 821–826.
(4) Zimmler, M. A.; Bao, J.; Capasso, F.; Müller, S.; Ronning, C. *Appl. Phys. Lett.* **2008**, *93*, 051101.
(5) Hsueh, T.; Chang, S.; Hsu, C.; Lin, Y.; Chen, I. *Appl. Phys. Lett.* **2007**, *91*, 053111.
(6) Hongsith, N.; Viriyaworasakul, C.; Mangkorntong, P.; Mangkorntong, N.; Choopun, S. *Ceram. Int.* **2008**, *34*, 823–826.
(7) Kim, S. W.; Fujita, S.; Fujita, S. *Appl. Phys. Lett.* **2005**, *86*, 153119.
(8) Willander, M.; Klason, P.; Yang, L. L.; Al-Hilli, S. M.; Zhao, Q. X.; Nur, O. *Phys. Status Solidi* **2008**, *5*, 3076–3083.
(9) Comini, E.; Baratto, C.; Faglia, G.; Ferroni, M.; Sberveglieri, G. *J. Phys. D: Appl. Phys.* **2007**, *40*, 7255–7259.
(10) Subannajui, K.; Kim, D. S.; Zacharias, M. *J. Appl. Phys.* **2008**, *104*, 014308.
(11) Özgür, U.; Alivov, Y. I.; Liu, C.; Teke, A.; Reshchikov, M. A.; Doğan, S.; Avrutin; Cho, S. J.; Morkoç, H. *J. Appl. Phys.* **2005**, *98*, 041301.
(12) Fan, H. J.; Bertram, F.; Dadgar, A.; Christen, J.; Krost, A.; Zacharias, M. *Nanotechnology* **2004**, *15*, 1401–1404.
(13) Fan, H. J.; Fleischer, F.; Lee, W.; Nielsch, K.; Scholz, R.; Zacharias, M.; Gösele, U.; Dadgar, A.; Krost, A. *Superlattices Microstruct.* **2004**, *36*, 95–105.
(14) Conley, J. F., Jr; Stecker, L.; Ono, Y. *Nanotechnology* **2005**, *16*, 292–296.
(15) Wang, J.; Sha, J.; Yang, Q.; Ma, X.; Zhang, H.; Yua, J.; Yang, D. *Mater. Lett.* **2005**, *59*, 2710–2714.
(16) Liao, X.; Zhang, X; Li, S. *Nanotechnology* **2008**, *19*, 225303.
(17) Dai, Y.; Zhang, Y.; Bai, Y. Q.; Wang, Z. L. *Chem. Phys. Lett.* **2003**, *375*, 96–101.
(18) Gardner, P. J.; Pang, P.; Preston, S. R. *J. Chem. Eng. Data* **1991**, *36*, 265–268.
(19) Yang, L.; Yang, J.; Wang, D.; Zhang, Y.; Wang, Y.; Liu, H.; Fan, H.; Lang *J. Phys. E* **2004**, *40*, 920–923.
(20) Craciun, V.; Amirhaghi, S.; Craciun, D.; Elders, J.; Gardeniers, J. G. E.; Boyd, I. W. *Appl. Surf. Sci.* **1995**, *86*, 99–106.
(21) Law, J. B. K.; Boothroyd, C. B.; Thong, J. T. L. *J. Cryst. Growth* **2008**, *310*, 2485–2492.